Effective Diffusion Transformer Architecture for Image Super-Resolution

Kun Cheng[1]*, Lei Yu[2]*, Zhijun Tu[2], Xiao He[1], Liyu Chen[2], Yong Guo[3],
Mingrui Zhu[1], Nannan Wang[1]†, Xinbo Gao[4], Jie Hu[2]

[1]State Key Laboratory of Integrated Services Networks, Xidian University
[2]Huawei Noah's Ark Lab
[3]Consumer Business Group, Huawei
[4]Chongqing Key Laboratory of Image Cognition, Chongqing University of Posts and Telecommunications

`kunncheng@stu.xidian.edu.cn, yulei96@huawei.com, nnwang@xidian.edu.cn`

Abstract

Recent advances indicate that diffusion models hold great promise in image super-resolution. While the latest methods are primarily based on latent diffusion models with convolutional neural networks, there are few attempts to explore transformers, which have demonstrated remarkable performance in image generation. In this work, we design an effective diffusion transformer for image super-resolution (DiT-SR) that achieves the visual quality of prior-based methods, but through a training-from-scratch manner. In practice, DiT-SR leverages an overall U-shaped architecture, and adopts a uniform isotropic design for all the transformer blocks across different stages. The former facilitates multi-scale hierarchical feature extraction, while the latter reallocates the computational resources to critical layers to further enhance performance. Moreover, we thoroughly analyze the limitation of the widely used AdaLN, and present a frequency-adaptive time-step conditioning module, enhancing the model's capacity to process distinct frequency information at different time steps. Extensive experiments demonstrate that DiT-SR outperforms the existing training-from-scratch diffusion-based SR methods significantly, and even beats some of the prior-based methods on pretrained Stable Diffusion, proving the superiority of diffusion transformer in image super-resolution.

1. Introduction

Image super-resolution (SR) aims to reconstruct a high-resolution (HR) image from a low-resolution (LR) input. Recently, diffusion models (DMs) [6, 16, 36] have demonstrated superior performance in image generation. Notable
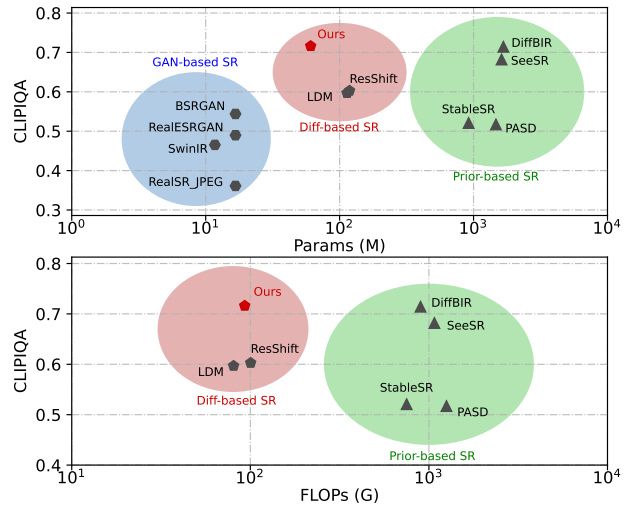

Figure 1. Comparisons between the proposed method and the latest SR methods on RealSR dataset. Top: CLIPIQA vs. Parameters. Bottom: CLIPIQA vs. FLOPs. Specifically, "Diff-based SR" refers to diffusion-based image super-resolution methods trained from scratch.

works [29, 45, 52, 56] have applied DMs to image super-resolution, achieving exceptional performance, particularly on complex natural scenes. Specifically, diffusion-based SR methods typically fall into two categories: the first group [36, 38, 39, 58] involves injecting LR images directly into the diffusion model and training it from scratch, while the second group [29, 45, 52, 55, 56], exploits the generative prior from pre-trained diffusion models, such as Stable Diffusion (SD) [35, 36], to enhance image super-resolution. Methods trained from scratch offer significant flexibility and ease of retraining following architectural modifications, making them ideal for lightweight applications. However, as

---

*Both authors contributed equally to this research.
†Corresponding author.

1

shown in Fig. 1, these methods typically struggle to match the upper bound performance of prior-based methods, which benefit from the rich generative prior gained through extensive training on vast datasets over thousands of GPU days. A natural question is can we develop a diffusion architecture trained from scratch while rivaling the performance of prior-based methods, balancing both performance and flexibility?

The advent of the Diffusion Transformer (DiT) [34] has made this idea feasible. This isotropic, full-transformer architecture, which maintains constant resolution and channel dimensions, shows remarkable performance and scalability, establishing a new paradigm in diffusion architecture design [3, 8, 9, 13, 27]. In contrast, early diffusion works [6, 16, 36] typically employed U-shaped denoiser architecture, which also remains popular in low-level tasks [50, 59] due to its hierarchical feature extraction capability and inductive bias conducive to denoising [51].

In this paper, we propose a diffusion transformer model for image super-resolution, namely DiT-SR. Instead of applying the standard diffusion transformer architecture directly, DiT-SR is a U-shape encoder-decoder network, but with isotropic designs for all the transformer blocks at different stages. Specifically, DiT-SR adopts the U-shaped global structure with incrementally wider channel dimensions at deeper layers, which helps recover more image details at multi-scale resolutions. Besides, inspired by the observations that (1) The transformer architecture with the same depth and channels could process tokens of different lengths well, *e.g.*, DiT-XL/2, DiT-XL/4 and DiT-XL/8. (2) High-resolution DiTs (*e.g.*, DiT/2) benefit more from scaling up than low-resolution DiTs (*e.g.*, DiT/8), thus we introduce the isotropic designs of DiT into the multi-scale framework. DiT-SR mandates the same channel number for all transformer modules in different stages, and sets the channel number bigger than the original setting of high resolution in U-Net, but much smaller than the low resolution. By allocating computational resource to critical layers, DiT-SR can greatly boost the capacity of the transformer architecture in multi-scale paradigms with the given computation budget.

Furthermore, we observe that DiT-based denoisers encounter a common issue [13] related to the inefficient mechanism of time-step conditioning. As illustrated in Fig. 2, the diffusion-based SR model attends to different frequency components at distinct denoising phases. Consequently, there should be a direct correlation between the time step and frequency. However, the widespreadly used Adaptive Layer Normalization (AdaLN), which modulates features solely in a channel-wise manner, does not effectively capture the unique temporal dynamics of the denoising process. To overcome this limitation, we propose an Adaptive Frequency Modulation (AdaFM) module, conditioning on the frequency domain. This highly efficient module, replacing AdaLN after each normalization layer, requires significantly fewer param-
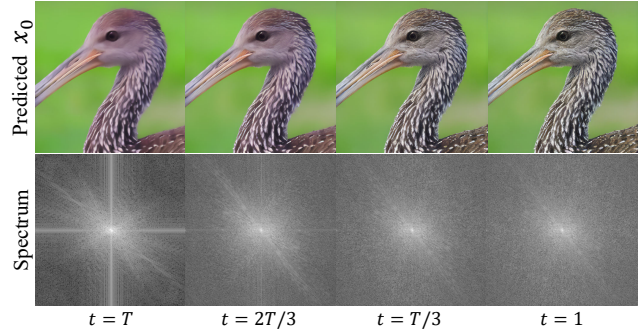

Figure 2. Analysis of images generated at different stages with a diffusion-based super-resolution model [58]. The first row shows the predicted clean images at various steps, while the second row displays the Fourier spectrums of each predicted clean image. The diffusion model initially generates low-frequency components (center part of spectrums) and subsequently generates high-frequency components (peripheral part of spectrums).

eters while boosting performance. The time step adaptively reweights different frequency components, making it especially suitable for image super-resolution, which necessitates a strong emphasis on high-frequency details.

We summarize the primary contributions as follows:
- We propose DiT-SR, a diffusion transformer specifically designed for image super-resolution, the first work that seamlessly combines the advantages of U-shaped and isotropic designs.
- We introduce an efficient yet effective frequency-wise time step conditioning module AdaFM, augmenting the diffusion model's ability to emphasize specific frequency information at varying time steps.
- Extensive experiments demonstrate that the proposed diffusion architecture outperforms existing training-from-scratch SR methods dramatically, and even surpasses some of prior-based SR methods with about only 5% of the parameters.

2. Related Works

2.1. Diffusion-based Image Super-Resolution

Recently, diffusion models [6, 16] have exhibited substantial benefits in image generation tasks, which generally fall into two categories: train-from-scratch methods and prior-based methods. SR3 [38] is the pioneer in introducing the diffusion model to the image super-resolution. LDM [36] enhances efficiency by performing the diffusion process in latent space. ResShift [58] reformulates the diffusion process resulting in a shortened Markov chain that reduces the number of denoising steps to 15. These methods offer significant flexibility and ease of retraining following architectural modifications, making them ideal for lightweight applications. Inspired by the remarkable potential of Stable Diffusion [35, 36]

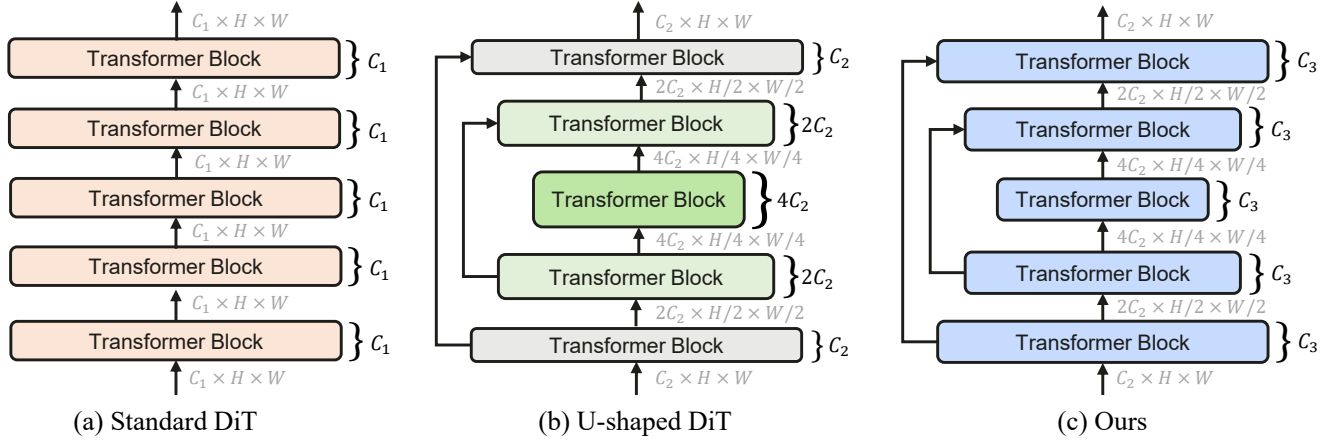(a) Standard DiT   (b) U-shaped DiT   (c) Ours

Figure 3. The comparison from the standard DiT to the proposed DiT-SR. (a): The standard DiT. (b):U-shaped DiT, incorporating downsampling and upsampling to standard DiT and increasing the channel dimension in deep layers. (c): The proposed DiT-SR. This architecture employs a U-shaped global structure, yet maintains the same channel dimension for all transformer blocks in different stages, allocating computational resource to high-resolution layers ($4C_2 > C_3 > C_2$) to boost the model capacity.

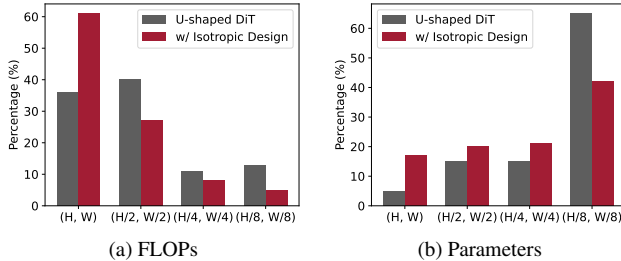(a) FLOPs   (b) Parameters

Figure 4. The percentage of FLOPs and parameters for each stage of the U-shaped DiT, both with and without isotropic design, show that more computational resources are allocated to high-resolution stages.

for text-to-image tasks, several methods [29, 45, 52, 55] have exploited its generative prior to guide real-world image super-resolution. While these prior-based methods yield remarkable results, their deployment is limited by slow inference speeds, which arise from the redundant denoiser architecture and the multi-step iterative denoising process. Despite SinSR [49] and AddSR [53] employing knowledge distillation for one-step denoising, their diffusion architectures typically cannot be altered without massive retraining. Orthogonal to the efforts to reduce denoising steps, we concentrate on developing an effective diffusion architecture trained from scratch while rivaling the performance of prior-based methods.

2.2. Diffusion Model Architecture

Previous diffusion studies [6, 16, 33, 36, 40] have predominantly utilized the U-Net [37] architecture for denoising, incorporating elements such as ResBlocks [14] and Transformer blocks [42]. DiT [34] marks a departure from the

U-shaped design by adopting an isotropic full transformer architecture, which showcases enhanced scalability. Subsequent works [9, 10, 13, 27, 31, 32] have adopted the standard DiT architecture and shown superior performance across various tasks. U-ViT [2] retains the long skip connections typical of U-Net but does not include upsampling or downsampling operations. Our proposed DiT architecture, which merges U-shaped and isotropic designs, achieves remarkable performance on image super-resolution.

3. Preliminaries

3.1. Diffusion Models

Given a LR image y and its corresponding HR image x_0, diffusion-based SR methods strive to model the conditional distribution $q(x_0|y)$. Typically, these methods define a T-step forward process that gradually introduce random noise to x_0, which can be succinctly achieved in one step through the reparameterization trick:

$$q\left(\boldsymbol{x_t}|\boldsymbol{x_0}\right) = \mathcal{N}\left(\boldsymbol{x_t}; \sqrt{\bar{\alpha}_t}\boldsymbol{x_0}, (1-\bar{\alpha}_t)\boldsymbol{I}\right) \text{ with } \bar{\alpha}_t = \prod_{i=0}^{t} \alpha_i,$$
(1)

where x_t denotes the noised image at time-step t and α_t is the predefined variance schedule. During the reverse process, the model starts from pure Gaussian noise and iteratively generates the preceding state x_{t-1} from x_t using the approximated posterior distribution:

$$p_\theta\left(\boldsymbol{x_{t-1}}|\boldsymbol{x_t}, \boldsymbol{y_0}\right) = \mathcal{N}\left(\boldsymbol{\mu_\theta}\left(\boldsymbol{x_t}, \boldsymbol{y_0}, t\right), \Sigma\left(\boldsymbol{x_t}, t\right)\right), \quad (2)$$

where $\Sigma(x_t, t)$ is a constant that depends on α_t, and $\mu_\theta(x_t, y_0, t)$ is parameterized by a denoiser $\epsilon_\theta(x_t, y_0, t)$.
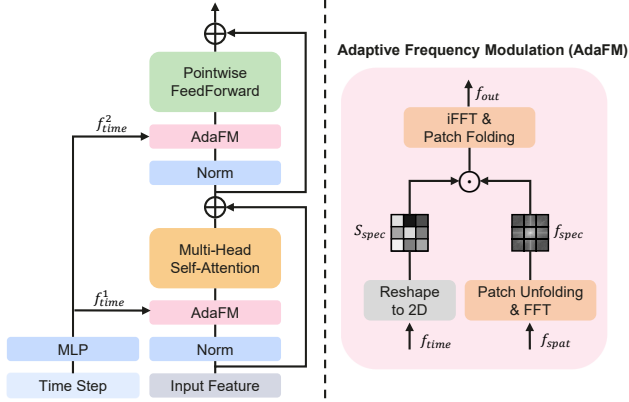
Figure 5. The illustration of transformer block in DiT-SR and Adaptive Frequency Modulation (AdaFM). AdaFM injects the time step into the frequency domain and adaptively reweights different frequency components.
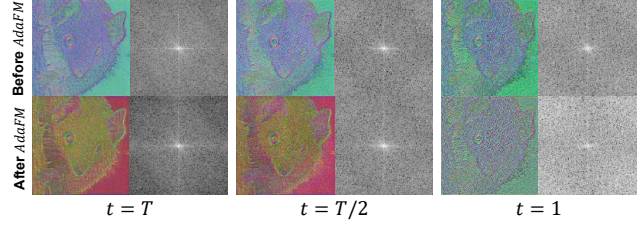

Figure 6. Visualization of the feature maps and their corresponding spectrums before and after applying AdaFM. AdaFM enhances the low-frequency components in the early stages of denoising (peripheral part of spectrums getting darker) and the high-frequency components in the later stages (peripheral part of spectrums getting brighter), thereby augmenting the diffusion model's ability to emphasize specific frequency at different time steps.

3.2. Residual Shifting

ResShift [58] constructs a Markov chain between HR and LR images rather than pure Gaussian noise. Let $e_0 = y_0 - x_0$ represents the resdual between the LR and HR images. Additionally, a shifting sequence $\{\eta_t\}_{t=1}^T$ is introduced, gradually increasing from $\eta_1 \to 0$ to $\eta_T \to 1$ with each timeste. The forward process is then formulated based on this shifting sequence:

$$q(x_t|x_0, y_0) = \mathcal{N}(x_t; x_0 + \eta_t e_0, \kappa^2 \eta_t I), \ t = 1, 2, \cdots, T, \tag{3}$$

where $\alpha_t = \eta_t - \eta_{t-1}$ for $t > 1$ and $\alpha_1 = \eta_1$. The hyperparameter κ controls the noise variance. The denoising process, $q(x_{t-1}|x_t, x_0, y_0)$ is formulated as follows:

$$p_\theta(x_{t-1}|x_t, x_0, y_0) = \mathcal{N}\left(x_{t-1} \left| \frac{\eta_{t-1}}{\eta_t} x_t + \frac{\alpha_t}{\eta_t} f_\theta(x_t, y_0, t), \kappa^2 \frac{\eta_{t-1}}{\eta_t} \alpha_t I \right.\right), \tag{4}$$

where x_0 is directly predicted by the denoiser $f_\theta(x_t, y_0, t)$. This well-designed transfer distribution for image super-resolution effectively reduces the length of Markov chains, thereby reducing the number of required time steps. We follow this paradigm to train our diffusion model.

4. Methodology

4.1. Overall Architecture

The proposed DiT-SR, depicted in Fig. 3, aims to be trained from scratch to potentially rival the performance of prior-based methods. This denoiser architecture features a U-shaped encoder-decoder global framework but with an isotropic design for all the transformer blocks at different stages. It includes several transformer stages in both the encoder and decoder, each with varying feature resolutions. Within each stage, multiple transformer blocks with uniform configurations are employed, reallocating computational resources to high-resolution layers to enhance the transformer architecture's capacity.

The LR image y and noisy image x_t are concatenated along the channel dimension, and together with the time step t, serve as inputs to the denoiser, which predicts x_0 and iteratively refines it as outlined in Eq. 4. As shown in Fig. 5, the transformer block consists of a multi-head self-attention (MHSA) mechanism [30] that operates as a spatial mixer, and a multi-layer perceptron (MLP) with two fully-connected layers separated by GELU activation, serving as channel mixers. Considering the high computational cost and memory constraints of global self-attention when processing high-resolution inputs, we employ local attention with window shifting as an alternative to the original self-attention [42]. Group normalization layers are applied before both the MHSA and MLP. Additionally, the proposed Adaptive Frequency Modulation (AdaFM) is integrated following each normalization layer to inject the time step. Our transformer block can be formulated as:

$$\begin{aligned} f_{time}^1, f_{time}^2 &= \mathrm{MLP_t}(t), \\ X &= \mathrm{MHSA}(\mathrm{AdaFM}(\mathrm{Norm}(X), f_{time}^1)) + X, \\ X &= \mathrm{MLP}(\mathrm{AdaFM}(\mathrm{Norm}(X), f_{time}^2)) + X. \end{aligned} \tag{5}$$

Subsequent sections will elaborate on the design motivation and specific details of DiT-SR, including the integration of U-shaped global architecture and isotropic block design, as well as the frequency-adaptive time-step conditioning mechanism.

4.2. Isotropic Design in U-shaped DiT

The U-Net architecture [37], with its encoder-decoder framework, is a popular choice for image generation and restoration tasks. Given the U-shaped architecture's multi-scale feature extraction ability, we propose integrating the U-shaped

Real-World Dataset

BSRGAN StableSR-200 DiffBIR-50 PASD-20 SeeSR-50

LR RealESRGAN SwinIR LDM-100 ResShift-15 Ours-15

Synthetic Dataset

BSRGAN StableSR-200 DiffBIR-50 PASD-20 SeeSR-50
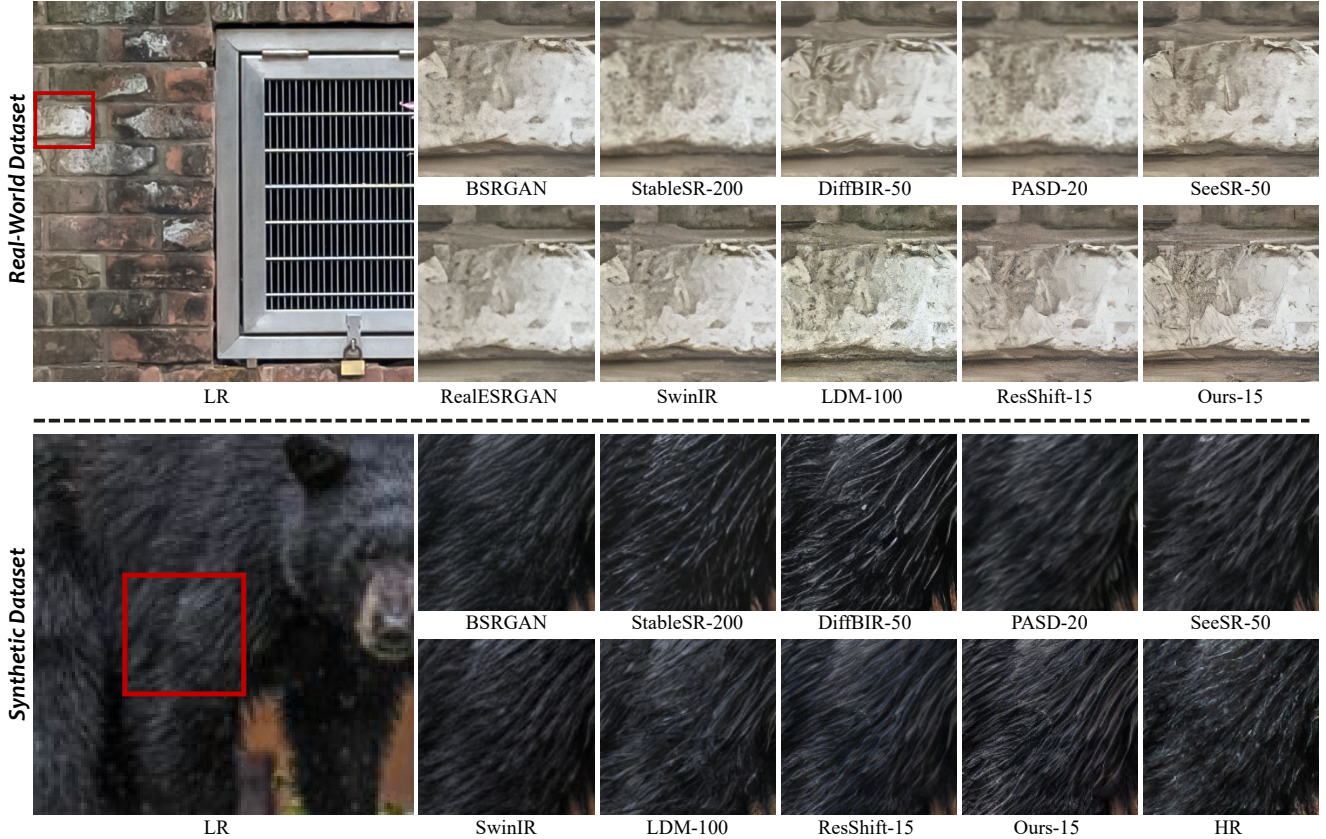
LR SwinIR LDM-100 ResShift-15 Ours-15 HR

Figure 7. Qualitative comparisons of different methods on both synthetic and real-world datasets.

global architecture into standard DiT to enhance its performance in image super-resolution. The encoder progressively reduces the resolutions of feature maps while increasing their channel dimensions, and the decoder reverses these operations for reconstruction.

We rethink the isotropic design in DiT and identify two notable characteristics. Firstly, DiTs with consistent channel and depth could effectively handle input with varying patch sizes (*e.g.*, DiT-XL/2, DiT-XL/4, and DiT-XL/8), which is analogous to processing different resolutions in U-Net. Secondly, DiTs at higher resolutions (*e.g.*, DiT/2) benefit more from scaling up compared to those at lower resolutions (*e.g.*, DiT/8). Motivated by these insights, we introduce this straightforward yet effective isotropic design to multi-scale U-shaped DiT in a pioneering way. Specifically, each transformer stage consists of several transformer blocks that operate at the same resolution. Within each stage, we standardize the inside feature's channel dimension to be the same across all stages, perform all the transformer blocks in reallocated feature space, and then reassemble them to their original dimensions. Considering that high-resolution stages capture more high-frequency details, which are crucial for image super-resolution and exhibit better scalability,

we set the standardized channel dimension larger than the original high-resolution stages in U-Net, yet considerably smaller than low-resolution stages. As depicted in Fig. 4, this isotropic principle allocates computational resources to critical high-resolution layers, avoiding the design of tedious scheduling policies, and greatly boosting the capacity of transformer architecture with far fewer parameters than conventional U-Net.

4.3. Frequency-Adaptive Time Step Conditioning

Since the diffusion model utilizes the same denoiser across various time steps, it is crucial to explicitly incorporate the time step as a condition. Adaptive Layer Normalization (AdaLN), first introduced in DiT [34], has been proven effective on image generation and is widely adopted in subsequent DiT-based models. Nevertheless, unlike image generation tasks, which start from pure noise and focus primarily on semantics, the SR task emphasizes the recovery of high-frequency details, necessitating the diffusion model to possess strong frequency perception capabilities.

Our investigation into the temporal evolution of images predicted by the diffusion-based super-resolution model reveals that it focuses on various frequency components at

Table 1. Performance and denoiser complexity comparison on real-world datasets. The best and second best results are highlighted in **bold** and <u>underline</u>. We denote the number of sampling steps for each diffusion-based method using the format "method-steps".

Methods	#Params	RealSR			RealSet65		
		CLIPIQA↑	MUSIQ↑	MANIQA↑	CLIPIQA↑	MUSIQ↑	MANIQA↑
GAN based Methods							
RealSR-JPEG	17M	0.3611	36.068	0.1772	0.5278	50.5394	0.2943
BSRGAN	17M	0.5438	63.5819	0.3685	0.616	65.5774	0.3897
RealESRGAN	17M	0.4898	59.6766	0.3679	0.5987	63.2228	0.3871
SwinIR	12M	0.4653	59.6316	0.3454	0.5778	63.8212	0.3816
Prior based Methods							
StableSR-200	919M	0.5207	59.4264	0.3563	0.5338	56.9207	0.3387
DiffBIR-50	1670M	<u>0.7142</u>	**66.843**	0.4802	**0.7398**	<u>69.7260</u>	<u>0.5000</u>
PASD-20	1469M	0.5170	58.4394	0.3682	0.5731	61.8813	0.3893
SeeSR-50	1619M	0.6819	<u>66.3461</u>	**0.5035**	0.7030	**68.9803**	**0.5084**
Training-from-Scratch Diff. based Methods							
LDM-100	114M	0.5969	55.4359	0.3071	0.5936	56.112	0.356
ResShift-15	119M	0.6028	58.8790	0.3891	0.6376	58.0400	0.4048
Ours-15	61M	**0.7161**	65.8334	<u>0.5022</u>	<u>0.7120</u>	66.7413	0.4821

different denoising stages. As shown in Fig. 2, the model initially reconstructs low-frequency elements, corresponding to the image structure, and progressively refines high-frequency details, associated with texture. Consequently, the time step should adaptively modulate different frequency components, using distinct modulation parameters for high and low-frequency regions. However, AdaLN modulates feature maps exclusively in the channel dimension, applying uniform modulation parameters across all spatial locations. This limitation hinders its ability to effectively address the specific frequency requirements of image super-resolution tasks. Moreover, it is challenging to generate modulation spatial-wise parameters from a one-dimensional time-step vector, as it requires adaptively distinguishing between the high and low-frequency components' spatial positions in the input image.

To solve this challenge, we introduce Adaptive Frequency Modulation (AdaFM), replacing AdaLN after each normalization layer and switching the time-step modulation from the spatial domain to the frequency domain, as shown in Fig. 5. Initially, to accommodate various input resolutions and enhance efficiency, we segment the spatial domain feature map $f_{spat} \in \mathbb{R}^{C \times H \times W}$ into $p \times p$ windows. Subsequently, we transform these segments into spectrograms $f_{spec} \in \mathbb{R}^{\frac{H \times W}{p^2} \times C \times p \times p}$ using the Fast Fourier Transform within each window. The time step is mapped to a p^2-dimensional vector f_{time} and reshaped into a frequency scale matrix $S_{spec} \in \mathbb{R}^{p \times p}$, which is then used to adaptively reweight various frequency components, thereby augmenting the diffusion model's ability to emphasize specific frequency at different time steps, as illustrated in Fig. 6.

In a spectrum, each pixel at a specific spatial position corresponds to a predetermined frequency component, defined solely by the feature map's spatial dimension, independent of its content. The frequency corresponding to a pixel located at spatial position (u, v) in spectrum $\in \mathbb{R}^{H \times W}$ can be formulated as:

$$f_u = \frac{u - H/2}{H} \times F_s, \quad f_v = \frac{v - W/2}{H} \times F_s, \quad (6)$$

where f_u, f_v denote the vertical and horizontal frequencies separately, and F_s indicates sampling frequency. This consistency allows the same frequency scale matrix S_{spec} to be applied across all windows and channels, significantly enhancing efficiency. In comparison to AdaLN, which requires $dim_{f_{time}} \times C \times 3 \times 2$ mapping parameters ($scale$, $shift$ and $gate$ for both self-attention and MLPs), AdaFM requires only $dim_{f_{time}} \times p^2 \times 2$. The process is formulated as follows:

$$\begin{aligned} S_{spec} &= \text{reshape}(f_{time}, p \times p), \\ f_{spec} &= \text{FFT}\left(\mathcal{P}\left(f_{spat}\right)\right), \\ f'_{spec} &= S_{spec} \odot f_{spec}, \\ f_{out} &= \mathcal{P}^{-1}\left(\text{iFFT}\left(f'_{spec}\right)\right), \end{aligned} \quad (7)$$

where $\mathcal{P}$ and $\mathcal{P}^{-1}$ denote the patch unfolding and folding operations, FFT and iFFT indicate Fast Fourier Transform and inverse Fourier Transform. Given that different frequencies correspond to distinct spatial locations on the feature map, the proposed frequency-wise time-step conditioning module actually provides spatial-wise modulation.

Table 2. Ablation Study on real-world datasets. The percentage reductions in the number of parameters and FLOPs are compared to the U-shaped DiT. The best results are highlighted in **bold**.

| Configuration | | #Params | FLOPs | RealSR | | RealSet65 | |
DiT Arch.	Time Conditioning			CLIPIQA↑	MUSIQ↑	CLIPIQA↑	MUSIQ↑
Isotropic	AdaLN	42.38M	122.99G	0.655	64.194	0.664	64.263
U-shape	AdaLN	264.39M	122.87G	0.688	64.062	0.693	65.604
Ours	AdaLN	100.64M(-62%)	93.11G(-24%)	0.700	64.676	0.699	**67.634**
Ours	AdaFM	60.79M(-77%)	93.03G(-24%)	**0.716**	**65.833**	**0.712**	66.741

5. Experiments

5.1. Experimental Settings

5.1.1 Datasets

We evaluate the proposed model on $\times 4$ real-world SR task. The training data comprises LSDIR [26], DIV2K [1], DIV8K [11], OutdoorSceneTraining [46], Flicker2K [41] and the first 10K face images from FFHQ [20] datasets. We partition LSDIR into a training set with 82991 images and a test set with 2000 images. Following LDM [36], HR images in our training set are randomly cropped to 256×256 and the degradation pipeline of RealESRGAN [48] is used to synthesize LR/HR pairs. The test set images are center-cropped to 512×512 and subjected to the same degradation pipeline used in the training stage to create a synthetic dataset, named LSDIR-Test. Furthermore, we utilize two real-world datasets: RealSR [4], which comprises 100 real images captured by Canon 5D3 and Nikon D810 cameras, and RealSet65 [58], including 65 low-resolution images collected from widely used datasets and the internet.

5.1.2 Implementation Details

Following LDM [36], the proposed architecture operates in latent space, utilizing the Vector Quantized GAN (VQ-GAN) [7] with a downsampling factor of 4. We train the proposed model for $300K$ iterations with a batch size of 64 using 8 NVIDIA Tesla V100 GPUs. The optimizer is Adam [23], and the learning rate is $5e^{-5}$. The FFT window size p is empirically set to 8 [24, 43]. Detailed architectural configurations are provided in the supplementary material.

5.1.3 Evaluation Metrics

We adopt reference-based metrics, including PSNR and LPIPS [61], to evaluate the performance of different models. Additionally, non-reference metrics such as CLIPIQA [44], MUSIQ [21], and MANIQA [54], which are more consistent with human perception in generative SR, are also employed. For assessments on real-world datasets, due to the lack of ground truth, we evaluate their performance using only non-reference metrics.

5.2. Comparison with State-of-the-Arts

5.2.1 Comparison Methods

We compared our proposed architecture with several latest SR methods, including GAN-based methods such as RealSR-JPEG[18], BSRGAN[60], RealESRGAN[48], and SwinIR[28], as well as diffusion-based methods like LDM[36], StableSR[45], ResShift[58], DiffBIR [29], PASD [55] and [52]. The steps are configured using their default settings. It is worth noting that StableSR, DiffBIR, PASD and SeeSR leverage the generative prior of Stable Diffusion, which is pretrained on large-scale datasets for thousands of GPU days, while LDM and ResShift are trained from scratch like ours.

5.2.2 Comparison on Real-World and Synthetic Datasets

We present the qualitative and quantitative results on Fig. 7, Tab. 1 and Tab. 3. The proposed architecture significantly outperforms existing training-from-scratch methods, and even surpasses competitive with state-of-the-art prior-based methods, while utilizing only about 5% of their parameters.

5.3. Ablation Study

5.3.1 U-shaped DiT with Isotropic Design

As described above, this paper proposes an evolutionary path from standard DiT to U-shaped DiT, and ultimately introduces isotropic design to multi-scale U-shaped DiT. We reimplement DiT for super-resolution, employing local attention with window shifting to replace the original self-attention. As shown in Table 2, the U-shaped DiT outperforms the standard DiT for the same FLOPs, but has six times more parameters. Notably, by reallocating computational resources to critical layers within the isotropic design, performance is improved even with a 62% reduction in parameters.

5.3.2 Adaptive-Frequency Modulation

The proposed AdaFM operates in the frequency domain, adaptively identifying high and low-frequency regions and modulating them separately with distinct parameters. Additionally, due to the nature of the frequency domain and our

Table 3. Performance comparison on the synthetic LSDIR-Test dataset. The best and second best results are highlighted in **bold** and underline.

Methods	LSDIR-Test				
	PSNR↑	LPIPS↓	CLIPIQA↑	MUSIQ↑	MANIQA↑
GAN based Methods					
RealSR-JPEG	22.16	0.360	0.546	59.02	0.342
BSRGAN	23.74	0.274	0.570	67.94	0.394
RealESRGAN	23.15	0.259	0.568	68.23	0.414
SwinIR	23.17	0.247	0.598	68.20	0.414
Prior based Methods					
StableSR-200	22.68	0.267	0.660	68.91	0.416
DiffBIR-50	22.84	0.274	0.709	70.05	0.455
PASD-20	23.57	0.279	0.624	69.07	0.440
SeeSR-50	22.90	0.251	**0.718**	**72.47**	**0.559**
Training-from-Scratch Diff. based Methods					
LDM-100	23.34	0.255	0.601	66.84	0.413
ResShift-15	**23.83**	0.247	0.640	67.74	0.464
Ours-15	23.60	**0.244**	0.646	69.32	0.483

highly efficient design, the parameter count of AdaFM is only a fraction of that of AdaLN. As shown in Tab. 2, replacing AdaLN with AdaFM reduced the number of denoiser parameters from 100.64M to 60.79M, while also enhancing model performance, demonstrating the effectiveness of AdaFM. Fig. 6 visualizes the feature maps and their spectrums before and after AdaFM, illustrating how it adaptively enhances low-frequency components in the early stages of denoising and high-frequency components in the later stages, thereby establishing a correlation between the time step and frequency.

6. Discussion and Conclusion

In this work, we introduce DiT-SR, an effective diffusion transformer architecture for image super-resolution that can be trained from scratch to rival the performance of prior-based methods. It integrates U-shaped global architecture and isotropic block designs, reallocating the computational resources to critical high-resolution layers, and boosting the performance efficiently. Furthermore, we propose an efficient yet effective time-step conditioning module AdaFM that adaptively reweights different frequency components, augmenting the diffusion model's ability to emphasize specific frequency information at varying time steps.

Future Work. AdaFM holds the potential to establish a new time-step conditioning paradigm for diffusion models, extending its application to various low-level visual tasks and even to text-to-image generation that also adheres to the paradigm of initially generating low frequencies followed by high frequencies.

Limitation and Ethical Statement. Due to differences in tasks and limited data, image super-resolution models typically do not exhibit the same level of scalability as text-to-image models. Although our denoiser achieves competitive performance with much fewer parameters compared to prior-based models, it still has some way to go before fully surpassing their performance. Similar to other content generation methods, our approach must be used cautiously to prevent potential misuse.

References

[1] Eirikur Agustsson and Radu Timofte. Ntire 2017 challenge on single image super-resolution: Dataset and study. In *The IEEE Conference on Computer Vision and Pattern Recognition (CVPR) Workshops*, 2017. 7

[2] Fan Bao, Shen Nie, Kaiwen Xue, Yue Cao, Chongxuan Li, Hang Su, and Jun Zhu. All are worth words: A vit backbone for diffusion models. In *Proceedings of the IEEE/CVF conference on computer vision and pattern recognition*, pages 22669–22679, 2023. 3

[3] Tim Brooks, Bill Peebles, Connor Holmes, Will DePue, Yufei Guo, Li Jing, David Schnurr, Joe Taylor, Troy Luhman, Eric Luhman, Clarence Ng, Ricky Wang, and Aditya Ramesh. Video generation models as world simulators. 2024. 2

[4] Jianrui Cai, Hui Zeng, Hongwei Yong, Zisheng Cao, and Lei Zhang. Toward real-world single image super-resolution: A new benchmark and a new model. In *Proceedings of the IEEE/CVF international conference on computer vision*, pages 3086–3095, 2019. 7

[5] Chaofeng Chen, Xiaoming Li, Lingbo Yang, Xianhui Lin, Lei Zhang, and Kwan-Yee K Wong. Progressive semantic-aware style transformation for blind face restoration. In *Proceedings of the IEEE/CVF conference on computer vision and pattern recognition*, pages 11896–11905, 2021. 12

[6] Prafulla Dhariwal and Alexander Nichol. Diffusion models beat gans on image synthesis. *Advances in neural information processing systems*, 34:8780–8794, 2021. 1, 2, 3

[7] Patrick Esser, Robin Rombach, and Bjorn Ommer. Taming transformers for high-resolution image synthesis. In *Proceedings of the IEEE/CVF conference on computer vision and pattern recognition*, pages 12873–12883, 2021. 7, 12

[8] Patrick Esser, Sumith Kulal, Andreas Blattmann, Rahim Entezari, Jonas Müller, Harry Saini, Yam Levi, Dominik Lorenz, Axel Sauer, Frederic Boesel, et al. Scaling rectified flow transformers for high-resolution image synthesis. In *Forty-first International Conference on Machine Learning*, 2024. 2

[9] Peng Gao, Le Zhuo, Ziyi Lin, Chris Liu, Junsong Chen, Ruoyi Du, Enze Xie, Xu Luo, Longtian Qiu, Yuhang Zhang, et al. Lumina-t2x: Transforming text into any modality, resolution, and duration via flow-based large diffusion transformers. *arXiv preprint arXiv:2405.05945*, 2024. 2, 3

[10] Shanghua Gao, Pan Zhou, Ming-Ming Cheng, and Shuicheng Yan. Mdtv2: Masked diffusion transformer is a strong image synthesizer. *arXiv preprint arXiv:2303.14389*, 2023. 3

[11] Shuhang Gu, Andreas Lugmayr, Martin Danelljan, Manuel Fritsche, Julien Lamour, and Radu Timofte. Div8k: Diverse 8k resolution image dataset. In *2019 IEEE/CVF International Conference on Computer Vision Workshop (ICCVW)*, pages 3512–3516. IEEE, 2019. 7

[12] Yuchao Gu, Xintao Wang, Liangbin Xie, Chao Dong, Gen Li, Ying Shan, and Ming-Ming Cheng. Vqfr: Blind face restoration with vector-quantized dictionary and parallel decoder. In *European Conference on Computer Vision*, pages 126–143. Springer, 2022. 12

[13] Ali Hatamizadeh, Jiaming Song, Guilin Liu, Jan Kautz, and Arash Vahdat. Diffit: Diffusion vision transformers for image generation. *arXiv preprint arXiv:2312.02139*, 2023. 2, 3

[14] Kaiming He, Xiangyu Zhang, Shaoqing Ren, and Jian Sun. Deep residual learning for image recognition. In *Proceedings of the IEEE conference on computer vision and pattern recognition*, pages 770–778, 2016. 3

[15] Martin Heusel, Hubert Ramsauer, Thomas Unterthiner, Bernhard Nessler, and Sepp Hochreiter. Gans trained by a two time-scale update rule converge to a local nash equilibrium. *Advances in neural information processing systems*, 30, 2017. 12

[16] Jonathan Ho, Ajay Jain, and Pieter Abbeel. Denoising diffusion probabilistic models. *Advances in neural information processing systems*, 33:6840–6851, 2020. 1, 2, 3, 12

[17] Gary B Huang, Marwan Mattar, Tamara Berg, and Eric Learned-Miller. Labeled faces in the wild: A database forstudying face recognition in unconstrained environments. In *Workshop on faces in'Real-Life'Images: detection, alignment, and recognition*, 2008. 12

[18] Xiaozhong Ji, Yun Cao, Ying Tai, Chengjie Wang, Jilin Li, and Feiyue Huang. Real-world super-resolution via kernel estimation and noise injection. In *proceedings of the IEEE/CVF conference on computer vision and pattern recognition workshops*, pages 466–467, 2020. 7

[19] Tero Karras, Timo Aila, Samuli Laine, and Jaakko Lehtinen. Progressive growing of gans for improved quality, stability, and variation. *arXiv preprint arXiv:1710.10196*, 2017. 12

[20] Tero Karras, Samuli Laine, and Timo Aila. A style-based generator architecture for generative adversarial networks. In *Proceedings of the IEEE/CVF conference on computer vision and pattern recognition*, pages 4401–4410, 2019. 7, 12

[21] Junjie Ke, Qifei Wang, Yilin Wang, Peyman Milanfar, and Feng Yang. Musiq: Multi-scale image quality transformer. In *Proceedings of the IEEE/CVF international conference on computer vision*, pages 5148–5157, 2021. 7, 12

[22] Bo-Kyeong Kim, Hyoung-Kyu Song, Thibault Castells, and Shinkook Choi. Bk-sdm: Architecturally compressed stable diffusion for efficient text-to-image generation. *ICML Workshop on Efficient Systems for Foundation Models (ES-FoMo)*, 2023. 11

[23] Diederik P Kingma and Jimmy Ba. Adam: A method for stochastic optimization. *arXiv preprint arXiv:1412.6980*, 2014. 7

[24] Lingshun Kong, Jiangxin Dong, Jianjun Ge, Mingqiang Li, and Jinshan Pan. Efficient frequency domain-based transformers for high-quality image deblurring. In *Proceedings of the IEEE/CVF Conference on Computer Vision and Pattern Recognition*, pages 5886–5895, 2023. 7

[25] Xiaoming Li, Chaofeng Chen, Shangchen Zhou, Xianhui Lin, Wangmeng Zuo, and Lei Zhang. Blind face restoration via deep multi-scale component dictionaries. In *European conference on computer vision*, pages 399–415. Springer, 2020. 12

[26] Yawei Li, Kai Zhang, Jingyun Liang, Jiezhang Cao, Ce Liu, Rui Gong, Yulun Zhang, Hao Tang, Yun Liu, Denis Demandolx, et al. Lsdir: A large scale dataset for image restoration. In *Proceedings of the IEEE/CVF Conference on Computer Vision and Pattern Recognition*, pages 1775–1787, 2023. 7

[27] Zhimin Li, Jianwei Zhang, Qin Lin, Jiangfeng Xiong, Yanxin Long, Xinchi Deng, Yingfang Zhang, Xingchao Liu, Minbin Huang, Zedong Xiao, et al. Hunyuan-dit: A powerful multi-resolution diffusion transformer with fine-grained chinese understanding. *arXiv preprint arXiv:2405.08748*, 2024. 2, 3

[28] Jingyun Liang, Jiezhang Cao, Guolei Sun, Kai Zhang, Luc Van Gool, and Radu Timofte. Swinir: Image restoration using swin transformer. In *Proceedings of the IEEE/CVF international conference on computer vision*, pages 1833–1844, 2021. 7, 11

[29] Xinqi Lin, Jingwen He, Ziyan Chen, Zhaoyang Lyu, Bo Dai, Fanghua Yu, Wanli Ouyang, Yu Qiao, and Chao Dong. Diffbir: Towards blind image restoration with generative diffusion prior, 2024. 1, 3, 7

[30] Ze Liu, Yutong Lin, Yue Cao, Han Hu, Yixuan Wei, Zheng Zhang, Stephen Lin, and Baining Guo. Swin transformer: Hierarchical vision transformer using shifted windows. In *Proceedings of the IEEE/CVF international conference on computer vision*, pages 10012–10022, 2021. 4

[31] Zeyu Lu, Zidong Wang, Di Huang, Chengyue Wu, Xihui Liu, Wanli Ouyang, and Lei Bai. Fit: Flexible vision transformer for diffusion model. *arXiv preprint arXiv:2402.12376*, 2024. 3

[32] Nanye Ma, Mark Goldstein, Michael S Albergo, Nicholas M Boffi, Eric Vanden-Eijnden, and Saining Xie. Sit: Exploring flow and diffusion-based generative models with scalable interpolant transformers. *arXiv preprint arXiv:2401.08740*, 2024. 3

[33] Alexander Quinn Nichol and Prafulla Dhariwal. Improved denoising diffusion probabilistic models. In *International conference on machine learning*, pages 8162–8171. PMLR, 2021. 3

[34] William Peebles and Saining Xie. Scalable diffusion models with transformers. In *Proceedings of the IEEE/CVF International Conference on Computer Vision*, pages 4195–4205, 2023. 2, 3, 5

[35] Dustin Podell, Zion English, Kyle Lacey, Andreas Blattmann, Tim Dockhorn, Jonas Müller, Joe Penna, and Robin Rombach. Sdxl: Improving latent diffusion models for high-resolution image synthesis. *arXiv preprint arXiv:2307.01952*, 2023. 1, 2

[36] Robin Rombach, Andreas Blattmann, Dominik Lorenz, Patrick Esser, and Björn Ommer. High-resolution image synthesis with latent diffusion models. In *Proceedings of the IEEE/CVF conference on computer vision and pattern recognition*, pages 10684–10695, 2022. 1, 2, 3, 7

[37] Olaf Ronneberger, Philipp Fischer, and Thomas Brox. U-net: Convolutional networks for biomedical image segmentation. In *Medical image computing and computer-assisted intervention–MICCAI 2015: 18th international conference,*

Munich, Germany, October 5-9, 2015, proceedings, part III 18, pages 234–241. Springer, 2015. 3, 4

[38] Chitwan Saharia, Jonathan Ho, William Chan, Tim Salimans, David J Fleet, and Mohammad Norouzi. Image super-resolution via iterative refinement. *IEEE transactions on pattern analysis and machine intelligence*, 45(4):4713–4726, 2022. 1, 2

[39] Shuyao Shang, Zhengyang Shan, Guangxing Liu, LunQian Wang, XingHua Wang, Zekai Zhang, and Jinglin Zhang. Resdiff: Combining cnn and diffusion model for image super-resolution. In *Proceedings of the AAAI Conference on Artificial Intelligence*, pages 8975–8983, 2024. 1

[40] Jiaming Song, Chenlin Meng, and Stefano Ermon. Denoising diffusion implicit models. *arXiv preprint arXiv:2010.02502*, 2020. 3

[41] Radu Timofte, Eirikur Agustsson, Luc Van Gool, Ming-Hsuan Yang, and Lei Zhang. Ntire 2017 challenge on single image super-resolution: Methods and results. In *Proceedings of the IEEE conference on computer vision and pattern recognition workshops*, pages 114–125, 2017. 7

[42] Ashish Vaswani, Noam Shazeer, Niki Parmar, Jakob Uszkoreit, Llion Jones, Aidan N Gomez, Łukasz Kaiser, and Illia Polosukhin. Attention is all you need. *Advances in neural information processing systems*, 30, 2017. 3, 4

[43] Gregory K Wallace. The jpeg still picture compression standard. *Communications of the ACM*, 34(4):30–44, 1991. 7

[44] Jianyi Wang, Kelvin CK Chan, and Chen Change Loy. Exploring clip for assessing the look and feel of images. In *Proceedings of the AAAI Conference on Artificial Intelligence*, pages 2555–2563, 2023. 7, 12

[45] Jianyi Wang, Zongsheng Yue, Shangchen Zhou, Kelvin CK Chan, and Chen Change Loy. Exploiting diffusion prior for real-world image super-resolution. *arXiv preprint arXiv:2305.07015*, 2023. 1, 3, 7

[46] Xintao Wang, Ke Yu, Chao Dong, and Chen Change Loy. Recovering realistic texture in image super-resolution by deep spatial feature transform. In *Proceedings of the IEEE conference on computer vision and pattern recognition*, pages 606–615, 2018. 7

[47] Xintao Wang, Yu Li, Honglun Zhang, and Ying Shan. Towards real-world blind face restoration with generative facial prior. In *Proceedings of the IEEE/CVF conference on computer vision and pattern recognition*, pages 9168–9178, 2021. 12

[48] Xintao Wang, Liangbin Xie, Chao Dong, and Ying Shan. Real-esrgan: Training real-world blind super-resolution with pure synthetic data. In *Proceedings of the IEEE/CVF international conference on computer vision*, pages 1905–1914, 2021. 7

[49] Yufei Wang, Wenhan Yang, Xinyuan Chen, Yaohui Wang, Lanqing Guo, Lap-Pui Chau, Ziwei Liu, Yu Qiao, Alex C Kot, and Bihan Wen. Sinsr: Diffusion-based image super-resolution in a single step. *arXiv preprint arXiv:2311.14760*, 2023. 3, 11

[50] Zhendong Wang, Xiaodong Cun, Jianmin Bao, Wengang Zhou, Jianzhuang Liu, and Houqiang Li. Uformer: A general u-shaped transformer for image restoration. In *Proceedings*

of the IEEE/CVF conference on computer vision and pattern recognition, pages 17683–17693, 2022. 2

[51] Christopher Williams, Fabian Falck, George Deligiannidis, Chris C Holmes, Arnaud Doucet, and Saifuddin Syed. A unified framework for u-net design and analysis. *Advances in Neural Information Processing Systems*, 36, 2024. 2

[52] Rongyuan Wu, Tao Yang, Lingchen Sun, Zhengqiang Zhang, Shuai Li, and Lei Zhang. Seesr: Towards semantics-aware real-world image super-resolution. In *Proceedings of the IEEE/CVF conference on computer vision and pattern recognition*, pages 25456–25467, 2024. 1, 3, 7

[53] Rui Xie, Ying Tai, Kai Zhang, Zhenyu Zhang, Jun Zhou, and Jian Yang. Addsr: Accelerating diffusion-based blind super-resolution with adversarial diffusion distillation. *arXiv preprint arXiv:2404.01717*, 2024. 3

[54] Sidi Yang, Tianhe Wu, Shuwei Shi, Shanshan Lao, Yuan Gong, Mingdeng Cao, Jiahao Wang, and Yujiu Yang. Maniqa: Multi-dimension attention network for no-reference image quality assessment. In *Proceedings of the IEEE/CVF Conference on Computer Vision and Pattern Recognition*, pages 1191–1200, 2022. 7, 12

[55] Tao Yang, Rongyuan Wu, Peiran Ren, Xuansong Xie, and Lei Zhang. Pixel-aware stable diffusion for realistic image super-resolution and personalized stylization. In *arXiv:2308.14469v3*, 2023. 1, 3, 7

[56] Fanghua Yu, Jinjin Gu, Zheyuan Li, Jinfan Hu, Xiangtao Kong, Xintao Wang, Jingwen He, Yu Qiao, and Chao Dong. Scaling up to excellence: Practicing model scaling for photo-realistic image restoration in the wild, 2024. 1

[57] Zongsheng Yue and Chen Change Loy. Difface: Blind face restoration with diffused error contraction. *arXiv preprint arXiv:2212.06512*, 2022. 12

[58] Zongsheng Yue, Jianyi Wang, and Chen Change Loy. Resshift: Efficient diffusion model for image super-resolution by residual shifting. *Advances in Neural Information Processing Systems*, 36, 2024. 1, 2, 4, 7, 11, 12

[59] Syed Waqas Zamir, Aditya Arora, Salman Khan, Munawar Hayat, Fahad Shahbaz Khan, Ming-Hsuan Yang, and Ling Shao. Multi-stage progressive image restoration. In *Proceedings of the IEEE/CVF conference on computer vision and pattern recognition*, pages 14821–14831, 2021. 2

[60] Kai Zhang, Jingyun Liang, Luc Van Gool, and Radu Timofte. Designing a practical degradation model for deep blind image super-resolution. In *Proceedings of the IEEE/CVF International Conference on Computer Vision*, pages 4791–4800, 2021. 7

[61] Richard Zhang, Phillip Isola, Alexei A Efros, Eli Shechtman, and Oliver Wang. The unreasonable effectiveness of deep features as a perceptual metric. In *Proceedings of the IEEE conference on computer vision and pattern recognition*, pages 586–595, 2018. 7, 12

[62] Shangchen Zhou, Kelvin Chan, Chongyi Li, and Chen Change Loy. Towards robust blind face restoration with codebook lookup transformer. *Advances in Neural Information Processing Systems*, 35:30599–30611, 2022. 12

Table 4. Diffusion Architecture Hyper-parameters.

DiT Arch.	Time Conditioning	#Params	FLOPs	Number of Blocks	Channels	Reallocated Channel
Isotropic	AdaLN	42.38M	122.99G	[6,6,6,6,6]	160	-
U-shape	AdaLN	264.39M	122.87G	[6,6,6,6]	[160,320,320,640]	-
Ours	AdaLN	100.64M	93.11G	[6,6,6,6]	[160,320,320,640]	192
Ours	AdaFM	60.79M	93.03G	[6,6,6,6]	[160,320,320,640]	192
Ours-Lite	AdaFM	30.89M	49.17G	[4,4,4]	[128,256,256]	160

A. Architecture Details

In the main paper, we present several diffusion architectures, including the standard DiT with an isotropic design, the U-shaped DiT, and our proposed architecture, which combines a U-shaped global structure with an isotropic block design. For the standard DiT, we re-implemented it inspired by SwinIR's Residual Swin Transformer Block (RSTB) [28], where each stage includes a residual connection. In this architecture, the feature resolution and channel dimensions remain consistent across all stages. The U-shaped DiT incorporates spatial downsampling and upsampling, with channel dimensions increasing progressively as depth increases. This design choice results in a much higher parameter count for the U-shaped DiT compared to the standard DiT, even when both architectures have the same FLOPs. Our proposed architecture strategically expands channels in the high-resolution layers and compresses them in the low-resolution layers. By reallocating limited parameters to the most critical layers, this design maximizes performance, surpassing even the original model. This approach effectively balances computational resources and enhances the model's ability to capture and refine crucial high-frequency details, which are essential for tasks like image super-resolution. The transformer block number is set to 6 for each stage, and the base channel is configured to 160. For the U-shaped global architecture, there are 4 stages, with the channel increase factor set to $[1, 2, 2, 4]$. The specific architectural details are provided in Tab. 4.

B. Compressing the U-shaped DiT

As described in the main paper, our proposed architecture outperforms the U-shaped DiT with only 48% of the parameters. This surprising result raises the question of whether U-Net architectures might be overly redundant, potentially limiting their performance. To explore this, we applied two separate compression strategies to the U-shaped DiT, adjusting its depth and width. For depth compression, we reduced the number of transformer blocks from 6 to 4 per stage, creating a "Narrower U-DiT." For width compression, we decreased the base channel dimension from 160 to 144. Despite these relatively modest reductions in parameter count (approximately 20%), both strategies resulted in noticeable performance degradation, as shown in Tab. 5. This outcome

indicates that U-Net architecture with $d6c160$ configuration has not yet reached a point of redundancy. Furthermore, it supports the effectiveness of our approach, which reallocates computational resources to critical high-resolution layers, thereby achieving superior performance with fewer parameters.

C. Lightweight Version

Different from prior-based super-resolution methods, training-from-scratch methods offer significant flexibility and ease of retraining after architectural modifications. This adaptability makes them particularly well-suited for lightweight applications. In addition to the base version of our proposed model reported in the main paper, we also develop a lite version. As illustrated in Tab. 4, the number of transformer blocks is reduced from 6 to 4, and the base channel is reduced from 160 to 128 with the channel increase factor $[1, 2, 2]$. Inspired by BK-SDM[22], we also remove the deepest layer to further streamline the model. As shown in Tab. 6, even though our lightweight model has only 25% of the parameters compared to ResShift[58], a state-of-the-art diffusion-based SR method trained from scratch, it still significantly outperforms ResShift, further demonstrating the superior model capacity of our proposed diffusion architecture.

Notably, our method is orthogonal to existing step-distillation methods and can be combined to enhance inference efficiency. Specifically, we utilize SinSR [49] to distill the lightweight model from a 15-step denoising process to a single-step denoising process. After applying step distillation, the CLIPIQA and MUSIQ metrics improved, while the MANIQA metric showed a decline. Users can choose whether to distill the model to achieve single-step denoising based on the specific requirements of their application scenario.

D. More Visualization Results

We provide more real-world image super-resolution results in Fig. 8.

Table 5. The results of compressing U-shaped DiT on real-world datasets. The percentage reductions in the number of parameters and FLOPs are compared to the U-shaped DiT. The best results are highlighted in **bold**.

Methods	#Params	FLOPs	RealSR		RealSet65	
			CLIPIQA↑	MUSIQ↑	CLIPIQA↑	MUSIQ↑
U-shaped DiT	264.39M	122.87G	0.688	64.062	0.693	65.604
Shallower U-DiT	196.65M(-26%)	96.30G(-22%)	0.671	63.319	0.683	64.097
Narrower U-DiT	214.20M(-19%)	99.56G(-19%)	0.682	63.631	0.692	65.469
Ours w/ AdaLN	100.64M(-62%)	93.11G(-24%)	**0.700**	**64.676**	**0.699**	**67.634**

Table 6. The results of compressing U-shaped DiT on real-world datasets.

Methods	#Params	RealSR			RealSet65		
		CLIPIQA↑	MUSIQ↑	MANIQA↑	CLIPIQA↑	MUSIQ↑	MANIQA↑
LDM-100	114M	0.5969	55.4359	0.3071	0.5936	56.1120	0.3560
ResShift-15	119M	0.6028	58.8790	0.3891	0.6376	58.0400	0.4048
Ours-15	61M	0.7161	65.8334	0.5022	0.7120	66.7413	0.4821
Ours-Lite-15	31M	0.6670	63.0544	0.4565	0.6694	64.3387	0.4420
Ours-Lite-1	31M	0.6993	63.3759	0.4262	0.7092	64.8329	0.4299

E. Experiments on Blind Face Restoration

Training Details. We use FFHQ[20] dataset containing 70K high-quality (HQ) face images with a resolution of 1024 × 1024. Firstly we resized the HQ images into 512 × 512, and then processed a typical degradation pipeline [47] to synthesize the LQ images. The learning rate grows to 5e-5 in 5000 iterations, then gradually decays from 5e-5 to 2e-5 according to the annealing cosine schedule and training ends at 200K iterations. Following ResShift [58], we employ VQGAN [7] with a downsampling factor of 8. The diffusion step is set to 4. In addition to diffusion loss [16] in latent space, LPIPS [61] loss is also adopted in pixel space. The model is trained with a batch size of 64 using 8 NVIDIA Tesla V100 GPUs.

Test Datasets. We use 2000 HR images that randomly selected from the validation dataset of CelebA-HQ[19] as the test datasets and the corresponding LQ images are synthesized following GFPGAN [47]. Additionally, three typical real-world datasets, named LFW[17], WebPhoto[47], and WIDER[62] are used to evaluate the performance on different degrees of degradation. LFW is a widely used face recognition dataset comprising 1,711 face images collected from various real-world sources. It provides a standard benchmark for evaluating face recognition algorithms under natural, unconstrained conditions. WebPhoto consists of 407 face images obtained through web crawling. This dataset includes a diverse range of images, including some older photos with significant degradation. It offers a variety of visual content and poses challenges for large-scale image retrieval and clustering algorithms due to its diverse and sometimes low-quality images. WIDER includes a subset of 970 face images selected from the larger WIDER Face dataset. The subset features images with heavy degradation, including occlusions, variations in poses, scales, and lighting conditions. It serves as a robust benchmark for assessing the effectiveness of face restoration methods under challenging real-world scenarios.

Comparison Methods. We compare our method with eight recent blind face restoration methods, including DFDNet [25], PSFRGAN[5], GFPGAN[47], VQFR[12], CodeFormer[62], DifFace[57], and ResShift[58].

Evaluation Metrics. To comprehensively assess various methods, this study adopts several reference-based metrics including LPIPS [61], identity score (IDS), landmark distance (LMD), and FID [15]. Non-reference metrics such as CLIPIQA [44], MUSIQ [21], and MANIQA [54] are also employed.

Comparisons with State-of-the-Art Methods. Both synthetic dataset and real-world datasets are evaluated for blind face restoration. We present quantitative metrics in Table 7 Table 8. Furthermore, we provide several real-world blind face restoration examples in Fig. 10 and synthetic blind restoration face restoration examples in Fig. 9.
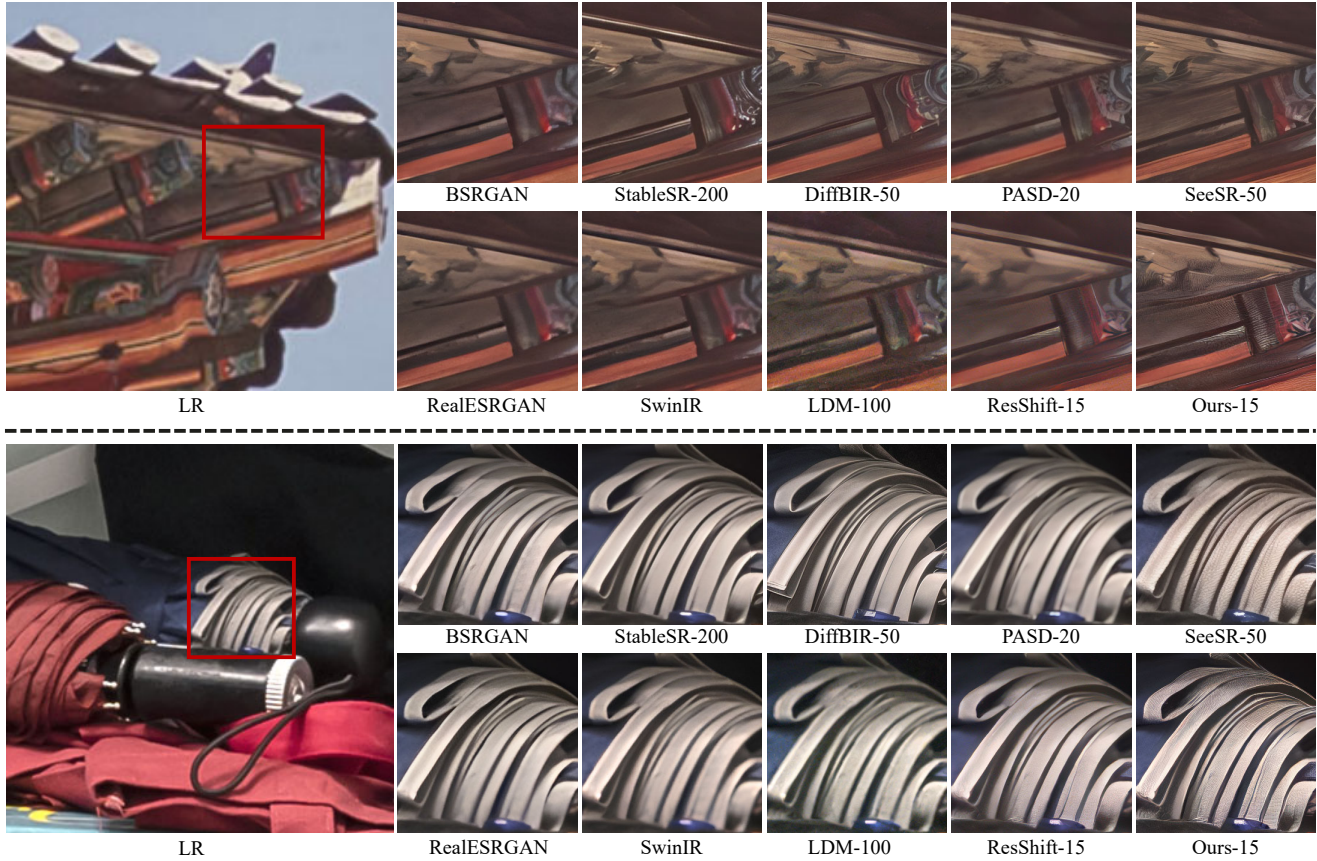
Figure 8. More visualization results on real-world datasets. Please zoom in for a better view.

Table 7. Quantitative results of different methods on the dataset of *CelebA-Test*. The best and second best results are highlighted in **bold** and <u>underline</u>.

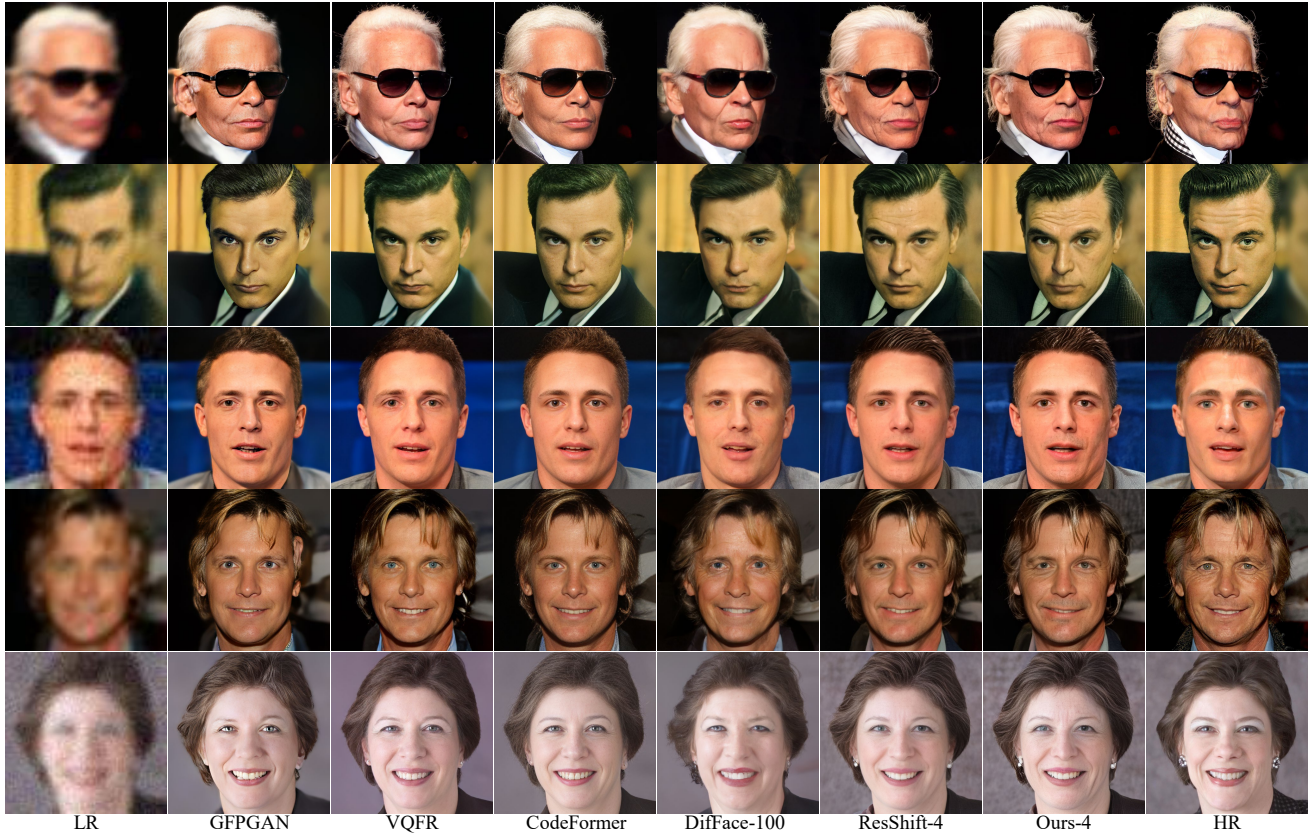| Methods	CelebA-Test						
	LPIPS↓	IDS↓	LMD↓	FID↓	CLIPIQA↑	MUSIQ↑	ManIQA
DFDNet	0.739	86.323	20.784	76.118	0.619	51.173	0.433
PSFRGAN	0.475	74.025	10.168	60.748	0.630	69.910	0.477
GFPGAN	0.416	66.820	8.886	27.698	0.671	75.388	<u>0.626</u>
VQFR	0.411	65.538	8.910	25.234	0.685	73.155	0.568
CodeFormer	<u>0.324</u>	**59.136**	**5.035**	26.160	<u>0.698</u>	**75.900**	0.571
DiffFace-100	0.338	63.033	5.301	23.212	0.527	66.042	0.475
ResShift-4	**0.309**	<u>59.623</u>	<u>5.056</u>	**17.564**	0.613	73.214	0.541
Ours-4	0.337	61.4644	5.235	<u>19.648</u>	**0.725**	<u>75.848</u>	**0.634**

Figure 9. Qualitative results of different methods on synthetic CelebA-Test dataset for blind face restoration. Please zoom in for a better view.

Table 8. Quantitative results of different methods on three real-world human face datasets. The best and second best results are highlighted in **bold** and <u>underline</u>.

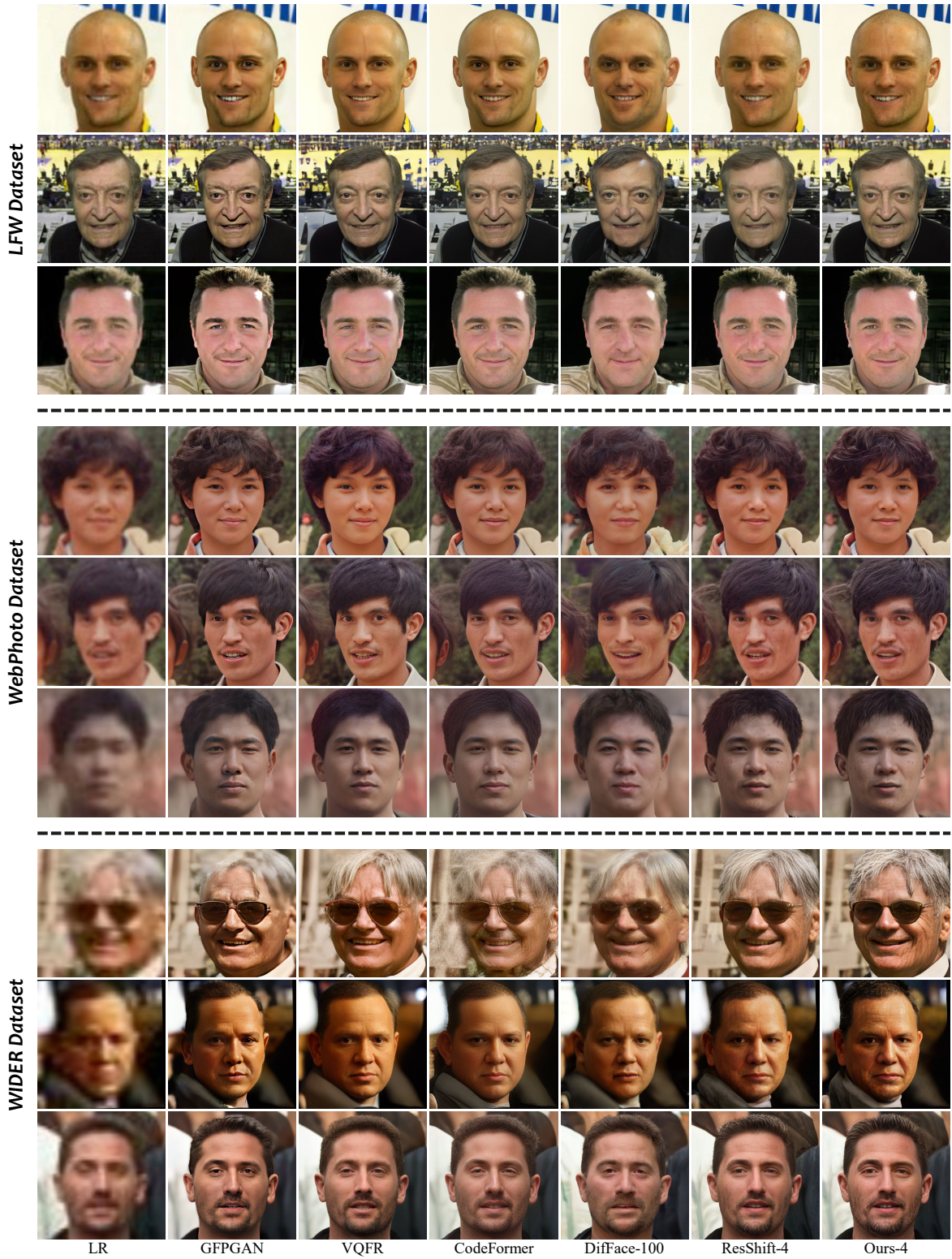| Methods	LFW			WebPhoto			Wider		
	CLIPIQA↑	MUSIQ↑	MANIQA↑	CLIPIQA↑	MUSIQ↑	MANIQA↑	CLIPIQA↑	MUSIQ↑	MANIQA↑
DFDNet	<u>0.716</u>	73.109	**0.6062**	0.654	69.024	0.550	0.625	63.210	0.514
PSFRGAN	0.647	73.602	0.5148	0.637	71.674	0.476	0.648	71.507	0.489
GFPGAN	0.687	<u>74.836</u>	<u>0.5908</u>	0.651	73.367	**0.577**	0.663	**74.694**	**0.602**
VQFR	0.710	74.386	0.5488	0.677	70.904	0.511	<u>0.707</u>	71.411	0.520
CoderFormer	0.689	**75.480**	0.5394	<u>0.692</u>	**74.004**	0.522	0.699	73.404	0.510
DiffFace-100	0.593	70.362	0.4716	0.555	65.379	0.436	0.561	64.970	0.436
ResShift-4	0.626	70.643	0.4893	0.621	71.007	0.495	0.629	71.084	0.494
Ours-4	**0.727**	73.187	0.564	**0.717**	<u>73.921</u>	<u>0.571</u>	**0.743**	<u>74.477</u>	<u>0.589</u>

Figure 10. Qualitative results of different methods on three real-world datasets for blind face restoration. Please zoom in for a better view.